Islamic Azad University

Journal of Optoelectronical Nanostructures

Journal homepage: https://sanad.iau.ir/journal/jopn

Research Paper

An Efficient Monte Carlo Model to Simulate the Electron Transport in Silicon-Based Devices

Mohammad Soroosh[1], Fatemeh Haddadan[2], Haraprasad Mondal[3], Sandip Swarnakar[4], Ehsan Adibnia[5], Mohammad Javad Maleki[1]

[1] Department of Electrical Engineering, Shahid Chamran University of Ahvaz, Ahvaz, Iran
[2] Department of Electrical Engineering, Karoon Institute of Higher Education, Ahvaz, Iran
[3] Department of Electronics and Communication Engineering, Dibrugarh University, Assam-786004, India
[4] Department of Electronics and Communication Engineering, Koneru Lakshmaiah Education Foundation, Vaddeswaram, Guntur-522302, Andhra Pradesh, India
[5] Faculty of Electrical and Computer Engineering, University of Sistan and Baluchestan (USB), P.O. Box 9816745563, Zahedan, Iran

Article History:
Received: 10.10.2025
Revised: 26.11.2025
Accepted: 26.11.2025
Published: 23.12.2025

Use your device to scan and read the article online

Keywords:
Boltzmann transport equation,
Electron scattering,
Monte Carlo method
Silicon

Abstract: This paper presents an efficient ensemble Monte Carlo approach for simulating electron transport in silicon-based semiconductors. The proposed model incorporates key scattering mechanisms—impurity, acoustic phonon, and nonpolar optical phonon interactions—by calculating their respective scattering rates, determining the probability of each scattering event, and assigning post-scattering energies and angles according to appropriate distributions. A three-valley framework is employed to account for anisotropy and conduction-band non-parabolicity, with direction-dependent effective masses and wave vectors, ensuring accurate simulation of electron transport under high electric fields. Key findings reveal fundamental transport characteristics: drift velocity shows linear dependence in weak fields, followed by saturation at higher fields due to increased scattering. Temperature increases cause reduced peak velocities and longer relaxation times, while higher impurity concentrations gradually decrease peak velocity through enhanced Coulombic scattering. Notably, significant velocity overshoot occurs at high fields (10-50 kV/cm), where electrons exhibit temporary velocity enhancements before stabilization. This arises from electrons entering high-energy states where momentum loss exceeds energy loss, with overshoot magnitude increasing with field strength. The study identifies a threshold field of ~30 kV/cm and validates results against Silvaco software (<5% deviation), experimental data, and other numerical methods. The model's novelty lies in capturing both steady-state and transient behaviors across varying temperatures, with the provided simulation code enhancing reproducibility. This framework offers robust analysis for designing high-speed silicon devices.

Citation: Mohammad Soroosh, Fatemeh Haddadan, Haraprasad Mondal, Sandip Swarnakar, Ehsan Adibnia, Mohammad Javad Maleki, An Efficient Monte Carlo Model to Simulate the Electron Transport in Silicon-Based Devices. **Journal of Optoelectronical Nanostructures.** 2025; 10 (4): 64-82

***Corresponding author:** Mohammad Soroosh
Address: Department of Electrical Engineering, Shahid Chamran University of Ahvaz, Ahvaz, Iran
Email: m.soroosh@scu.ac.ir
DOI: https://doi.org/10.71577/jopn.2025.1220725

1. INTRODUCTION

Silicon is the cornerstone of modern electronics, widely utilized in the production of semiconductors due to its unique physical and electrical properties [1]. Its abundance, excellent thermal stability, and ability to form a stable crystalline structure make it an essential material in devices [2-3] such as microchips [4-5], photonic crystal-based devices [6-9], and integrated circuits [10-12]. These components underpin technologies ranging from telecommunications [13] to highly compacted optical circuits [14-16], driving advancements in industries globally [17].

Understanding electron transport in silicon is fundamental to improving device performance. Electron transport is governed by various mechanisms, including scattering due to phonons, impurities, and defects within the silicon lattice [18]. These processes affect critical properties such as carrier mobility and conductivity [19]. Moreover, external factors such as electric fields and temperature variations further influence electron dynamics, making accurate modeling indispensable for semiconductor design [20].

Monte Carlo simulation is known as a powerful method to model and predict electron behavior in semiconductors [21]. Unlike deterministic methods, Monte Carlo simulations provide a probabilistic approach, capturing the stochastic nature of scattering events [22]. This method allows for detailed analysis of electron trajectories, offering insights into transport phenomena under different operational conditions, such as high electric fields and varying doping levels [23]. It has proven particularly effective in identifying non-linear behaviors that impact device efficiency [24-25].

A study employs Ensemble Monte Carlo simulations to investigate electron transport in GaAs quantum wires, revealing that the one-dimensional density of states enhances low-field mobility and increases high-field saturation velocity through anisotropic effects [26]. A report uses an Ensemble Monte Carlo simulator to solve the coupled Boltzmann–Poisson equations for electron transport in cubic GaN n+–n–n+ structures under applied voltages from 0.5 to 4 V. The model includes semiclassical carrier motion along with phonon and ionized-impurity scattering. Key transport quantities—such as electron density, velocity, kinetic energy, potential, and electric field—are evaluated for different lattice temperatures and active-layer lengths [27]. Another study performs ensemble Monte Carlo simulations to investigate electron transport in small-diameter semiconducting zigzag (n,0) carbon nanotubes using a tight-binding electronic structure. The simulations include key electron–phonon scattering mechanisms involving longitudinal acoustic and optical phonons and evaluate the

electron distribution in space and time [28]. A work employs an advanced EMC model to simulate electron behavior in InN, utilizing a detailed five-band model and a numerically computed impact ionization rate. The results reveal a substantially higher peak electron drift velocity than GaN, significant anisotropy in the velocity-field characteristic, and a low-field mobility within a specific range [29]. The proposed model offers several advantages over the first four studies. Unlike the earlier works that focus on specific materials such as GaAs, GaN, carbon nanotubes, and InN, this work presents a more general and versatile EMC framework for silicon-based semiconductors, incorporating a comprehensive three-valley model that captures anisotropy and conduction-band non-parabolicity more accurately. It also provides a far more detailed analysis of high-field transport—including clear characterization of velocity saturation, strong velocity overshoot, and a defined threshold field—while systematically examining the effects of temperature and impurity concentration on transport properties, which the previous studies address only partially. Furthermore, it demonstrates stronger validation through close agreement with Silvaco simulations, experimental data, and other numerical methods, and enhances reproducibility by providing its simulation code. Together, these features make this work a more complete and broadly applicable transport study compared to the previous works.

The Ensemble Monte Carlo method offers key advantages over the drift–diffusion (DD) model, particularly for nanoscale and high-field semiconductor devices. EMC provides a microscopic, particle-based simulation of individual carrier trajectories, allowing non-equilibrium effects such as velocity overshoot, ballistic transport, hot-carrier phenomena, and transient behavior to be captured with high fidelity, effects that the DD model, which assumes local equilibrium and uses averaged mobilities, cannot resolve [30]. Moreover, EMC naturally accommodates detailed physics such as full-band structure, anisotropy, non-parabolic dispersion, and complex scattering mechanisms while DD often relies on empirical parameterization and loses accuracy under extreme conditions [31]. Importantly, EMC has been shown to predict device variability more accurately; for example, in Si nanowire FETs, Monte Carlo simulations reveal ON-current fluctuations from line-edge roughness or metal-gate granularity that drift–diffusion models can overestimate by tens of percent [32]. Although computationally more demanding, EMC thus provides significantly greater predictive power and physical realism compared to the drift–diffusion approach.

The findings of this study can directly support the design of high-speed integrated circuits, and introducing a clear optoelectronic nanostructure as a

potential application further strengthens the relevance of the proposed EMC model. Given the model's ability to accurately capture electron dynamics under high electric fields and varying temperatures, it is well-suited for analyzing carrier transport in optoelectronic nanostructures such as silicon-based nanowire photodetectors or high-speed silicon modulators. These devices rely on fast carrier response and strong field-dependent transport properties, which the presented EMC framework can effectively predict and optimize. This study presents a new ensemble Monte Carlo model to solve the Boltzmann transport equation of electrons in silicon. By simulating scattering mechanisms and analyzing the effects of temperature, electric fields, and impurities, the research aims to provide an efficient and fundamental model for silicon-based devices. This model enables researchers to have a comprehensive understanding of transport dynamics. Such insights are pivotal for optimizing the design and functionality of semiconductor devices, ensuring greater energy efficiency and performance. The result shows the time-dependent response of electron drift velocity and energy under various applied electric fields.

2. THE PROPOSED MONTE CARLO METHOD

The Monte Carlo method is highly efficient in simulating any phenomenon with a random nature. The movement of electrons in a semiconductor is also inherently random. Given that the basis of electron transport in all semiconductors is the Boltzmann equation, solving this equation and obtaining the distribution function (f) becomes important. Because with f, other necessary quantities for studying electron transport in semiconductors can be obtained. The Boltzmann equation is defined as follows [33]:

$$\frac{\partial f}{\partial t} + V.\nabla_r f + k.\nabla_k f = \left(\frac{\partial f}{\partial t}\right)_{coll} \quad (1)$$

This equation cannot be solved analytically without making simplifications, but using the Monte Carlo method, which is the basis of this paper, the Boltzmann equation is solved stochastically over a time interval, and the distribution function is calculated accurately. In this method, computer-generated random numbers are used to estimate the desired quantities. For example, the relaxation time between collisions is obtained from the following relation [33]:

$$t_r = -\frac{1}{\Gamma} ln(r) \quad (2)$$

where r is a random number in the range 0 < r < 1, and Γ is the total scattering rate, meaning the relaxation time between collisions.

$$\Gamma_{\text{total}} = \Gamma_{\text{non-polar optical}} + \Gamma_{\text{acoustic}} + \Gamma_{\text{impurity}} \quad (3)$$

Initially, 50000 superparticles are distributed in the momentum space according to the Maxwell-Boltzmann statistics. Due to various scattering mechanisms within the material (including non-polar optical phonon scattering, inter-valley and intra-valley phonon scattering, acoustic phonon scattering, and impurity), their states change. Given the presence of strong electric fields in the calculations (greater than 1 kV/cm), the central valley should be considered non-parabolic, and its effect on the equation is as follows [23]:

$$E_k(1 + \alpha E_k) = \frac{\hbar^2 k^2}{2m^*} \quad (4)$$

where α is the non-parabolicity factor of the valley and m* is the effective mass of electrons. Due to the consideration of an elliptical band structure, the band structure becomes dependent on the crystal lattice directions, and both the effective mass and the wave vector become dependent on these directions. As a result, the above relations are modified as follows [23]:

$$E_k(1 + \alpha E_k) = \frac{\hbar^2}{2}\left[\frac{k_l^2}{m_l^*} + \frac{k_t^2}{m_t^*}\right] \quad (5)$$

where m_t^*, m_l^*, k_t^*, and k_l^* are the transverse and longitudinal masses, transverse and longitudinal wave vectors in the momentum space with an elliptical distribution, respectively.

Since a real crystal does not have a perfectly periodic structure, it is also considered the interaction of electrons with these defects. These defects include the absence of an atom from its original position or the substitution of an impurity atom in the lattice structure. Moreover, lattice vibrations also disturb the periodic potential and cause electron scattering. The effect of these defects is introduced into calculations as a perturbation potential according to quantum mechanics. The band and physical parameters related to Si are given; the bandgap, non-parabolicity coefficient, m_t^*/m_0, and m_l^*/m_0 are 1.12 eV, 0.5, 0.19, and 0.92, respectively [18]. Moreover, the density, dielectric constant, optical phonon energy, acoustic velocity, and deformed potential constant are 2329 kg/m3, 11.7,

0.063 eV, 9040 m/s, and 9 eV, respectively [18].

Silicon crystallizes in the diamond structure. Its band structure reveals that the conduction band minimum (bandgap) lies along the Δ and X directions in k-space. Due to the significant energy difference between these valleys and the lowest valley, most simulations consider only the central valley. This is justified by the negligible impact of higher valleys on properties such as electron mobility under typical operating conditions [18]. However, in specific studies sensitive to phenomena like inter-valley electron transfer, it may be necessary to consider all valleys.

In silicon semiconductors, electron scattering is primarily caused by interactions with phonons. These scattering events can be categorized into intra-valley and inter-valley scattering. In intra-valley scattering, electrons within the same valley of the band structure exchange energy with acoustic or optical phonons, leading to changes in their energy and momentum. Inter-valley scattering involves the transfer of electrons from one valley to another, typically accompanied by the absorption or emission of optical phonons. Due to the significant change in electron energy, these scattering events are inelastic. Phonon scattering has a significant impact on electron mobility and, consequently, on the electrical conductivity of the material.

Intra-valley scattering refers to the scattering of electrons within the central valley of the conduction band, primarily due to interactions with acoustic phonons. Because the energy of acoustic phonons is much lower than the thermal energy, this type of scattering can be approximated as elastic. This approximation assumes that the electron energy remains constant during the scattering event, simplifying the calculations [23]. Other scattering mechanisms, such as scattering by optical phonons, impurities, and other electrons, are typically considered inelastic, as electrons gain or lose significant energy during these scattering events.

In a semiconductor crystal, electrons are the primary charge carriers. Their movement through the crystal lattice can be disrupted by various factors, such as the coulomb force from atomic nuclei, impurity scattering, phonon scattering, acoustic phonons, and non-polar optical phonons. From a quantum mechanical perspective, these disruptive phenomena are viewed as perturbation potentials. These potentials lead to electron scattering, a fundamental process that impacts the electronic properties of semiconductors. The scattering rates due to impurities, acoustic phonons, and non-polar optical phonons are crucial parameters in determining the overall electrical behavior of a semiconductor device. These rates are often incorporated into a scattering matrix. Equation (6) in the reference [18]

likely provides a specific formula for calculating the impurity scattering rate.

By understanding these scattering mechanisms and their associated rates, scientists and engineers can optimize the design and performance of semiconductor devices.

$$W_{imp}(k) = \frac{2\pi N_I Z^2 q^4 N_S(E_k)}{\hbar \varepsilon_s^2} \frac{1}{L_D^2(4k^2 + L_D^2)} \quad (6)$$

$$N_s(E_k) = \frac{(2m^*)^{3/2}\sqrt{E_k}}{4\pi^2\hbar^3} \quad (7)$$

where k, E, ε, and L_D represent the momentum, energy of electrons, permittivity of material, and Debye length, respectively, while $N_s(E)$ and Z denote the density of states for electrons and the impurity charge, respectively.

To completely define the state of the electron after scattering, the scattering probability $W_{imp}(k)$, and the scattering angles φ and θ should be determined. The angle φ, being independent of the collision process, is randomly selected within the range 0 to 2π. To determine θ, $W_{imp}(\theta)/W_{imp}(k)$ is computed, establishing a relationship that depends on θ. Given the influence of the Debye length on cosθ, Equation (8) is used to calculate θ.

$$\cos\theta = 1 - \frac{2r}{1 + (1 - r)(\frac{2k}{L_D})^2} \quad (8)$$

where r is a symbol to generate a random number between 0 and 1. The scattering rate of acoustic phonons is defined by Equation (9), where Ξ_d, k′, and c_L show the deformation potential, the electron wave vector after scattering, and the elasticity constant, respectively. In this scattering, it is supposed that the collision is elastic, implying that the carrier's energy remains unchanged after the collision [18].

$$W_{aco}(k, k') = \frac{\pi \Xi_d^2 KT}{\hbar c_L} N_S(E_k) \quad (9)$$

Non-polar optical phonon scattering is defined as an inelastic process, including phonon energy compared to the environment's thermal energy. This type of scattering appears in two modes: intra-valley and inter-valley. In intervalley scattering, the need for a substantial change in momentum restricts the process to phonons whose wave vectors lie close to the edges of the Brillouin zone. The

phonon energy is slightly more than that at the center of the corresponding boundary region. The azimuthal angle φ is determined by producing a random number uniformly distributed between 0 and 2π, while the cosθ of the polar angle is achieved using a random number uniformly distributed from -1 to +1.

Equations (10) and (11) describe the scattering rates for intra-valley and inter-valley non-polar optical phonons, respectively, where D_0 represents the deformation potential, ω_0 denotes the angular frequency at equilibrium, and $\hbar\,\omega_0$ corresponds to the energy of the optical phonon. The sign ± indicates the two possible cases of phonon emission and absorption [18].

$$W^{intra}_{Non-POP}(k) = \frac{\pi D_o^2}{\rho\omega_o}(n_b + \frac{1}{2} \mp \frac{1}{2})N_s(E_k \pm \hbar\omega_o) \quad (10)$$

$$W^{inter}_{Non-POP}(k) = \frac{\pi D_{ij}^2 z_j}{\rho\omega_{ij}\Omega}(n_b(\omega_{ij}) + \frac{1}{2} \mp \frac{1}{2})N_s(E_k \pm \hbar\omega_{ij} - \Delta E_{ji}) \quad (11)$$

where Ω represents the volume of impurity, D_{ij} denotes the inter-valley deformation potential. After electrons are scattered, they can transition to other valleys, where z_j determines the number of valleys. ΔE_{ji} denotes the difference in the energy between the minimum energy of the two valleys, where the indices j and i correspond to the valleys associated with the electron after and before scattering, respectively.)

The number of phonons in the q_s state at equilibrium is determined by the Bose-Einstein distribution, as phonons are treated as bosonic particles. Equation (12) provides the expression for the phonon population. Here, n_b represents the number of similar bosonic particles that oscillate at frequency ω_{qs} with energy $\hbar\omega_{qs}$.

$$n_b(\omega_{qs}) = \frac{1}{\exp(\hbar\omega_{qs}/KT) - 1} \quad (12)$$

Figure 1 illustrates the geometry of the simulated device, the electron concentration in the valleys, and energy versus wavevector. In semiconductor physics, the energy-momentum (E-k) relationship of charge carriers (electrons) is often approximated as parabolic. This simplification leads to a constant effective mass, making theoretical calculations more straightforward. However, in reality, the band structure of many semiconductors deviates from this ideal parabolic shape, especially at higher energies. This non-parabolicity has significant implications for the electronic and optical properties of semiconductors. In the non-parabolic

band, the effective mass increases with increasing energy. This leads to a more complex carrier transport behavior, affecting scattering mechanisms.

3. THE SIMULATION RESULTS

Based on the proposed EMC model, the results of simulations in silicon semiconductors under various electric fields are presented. Figure 2 illustrates the electron drift velocity characteristics at a temperature of 300 K and an impurity concentration of 2×10^{17} cm^{-3} under steady-state conditions. As observed in figure 2, the electron drift velocity rises with increasing electric field. However, at a threshold field of approximately 30 kV/cm, the rate of velocity increase slows down, and eventually, the velocity saturates at a value on the order of the thermal velocity of electrons in silicon, which is approximately 10^5 m/s [32].

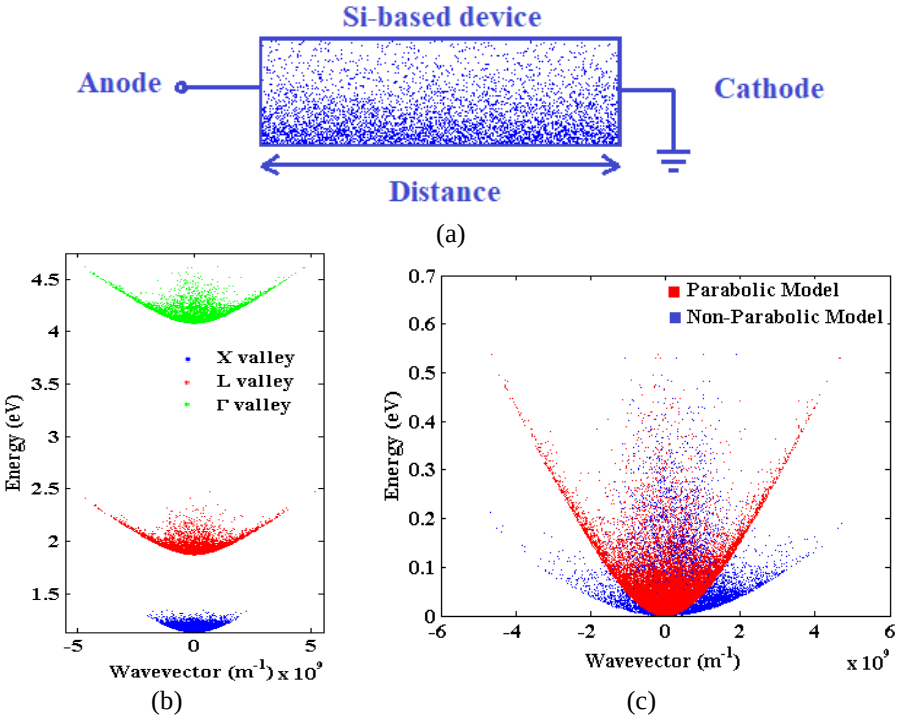

Fig. 1. (a) The geometry of the simulated device. The energy band diagram versus the wavevector of silicon (b) and electron concentration in the valleys (c) for two parabolic and non-parabolic cases

In weak electric fields, the drift velocity increases linearly with increasing electric field, where the slope of this line represents the electron mobility.

However, due to increased scattering events within the semiconductor as the electric field strength increases, which act as obstacles to electron motion, the velocity increase is hindered and eventually saturates. As shown in Figure 2, the results obtained from Monte Carlo simulations and Silvaco simulations exhibit good agreement. Accordingly, the simple MC model can be considered an efficient model to simulate silicon devices.

Significant attention has been given to electron transport within submicron devices due to their potential for high-frequency and high-speed applications. When the time it takes for electrons to traverse a device becomes similar to or shorter than the time it takes for electrons to reach a stable state (relaxation time), electrons injected into the device may not achieve their steady-state velocity during their journey through the device. Therefore, it's crucial to understand that the velocity-field relationships determined in earlier analyses may not accurately describe electron transport within submicron devices. The transient behavior observed after electron injection allows the average velocity to exceed the typical saturation value.

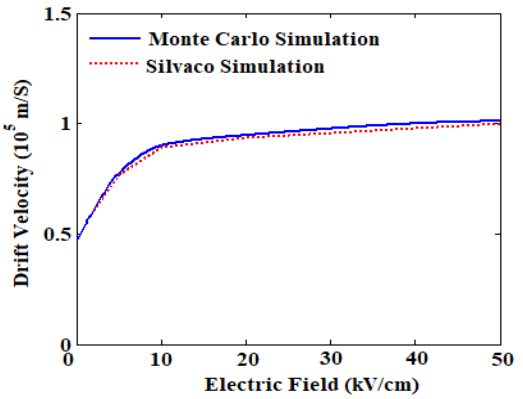

Fig. 2. Steady-state electron drift velocity as a function of applied electric field in Si semiconductor at 300 K

Figure 3 depicts the temporal response of electron drift velocity at three different temperatures: 300K, 400K, and 500K, under applied electric fields of 20 kV/cm and 50 kV/cm. The figure shows that as temperature increases, the peak of electron drift velocity decreases and shifts towards longer times. This behavior in the drift velocity curve is attributed to the increased probability of scattering events with increasing temperature.

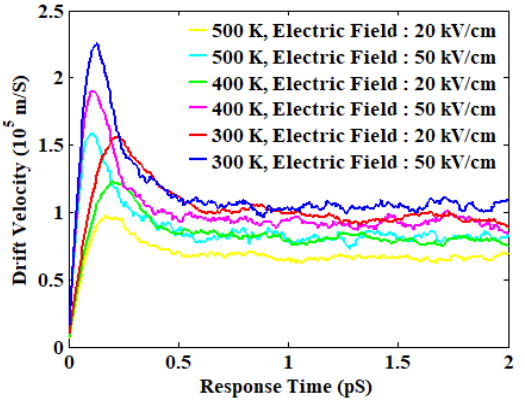

Fig. 3. The time-dependent changes of electron drift velocity with temperature

Figure 4 illustrates the temporal response of electrons for three different impurity concentrations: 2×10^{17} cm^{-3}, 5×10^{17} cm^{-3}, and 10^{18} cm^{-3}, under an applied electric field of 50 kV/cm. As observed in the figure, the peak velocity decreases gradually with increasing impurity concentration. This phenomenon is attributed to the fact that as the number of ionized impurity centers increases, electrons experience more frequent Coulombic scattering, resulting in an increased scattering rate due to ionized impurities and a consequent decrease in carrier velocity.

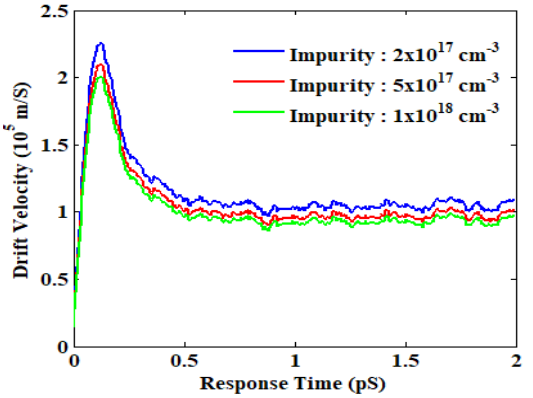

Fig. 4. The time-dependent change in electron drift velocity varies with changes in impurity density for a temperature of 300K

Figure 5 shows the time-dependent response of electron drift velocity and energy under various applied electric fields. As observed in figure 5(a), in fields

of 10 kV/cm, 20 kV/cm, and 50 kV/cm, peaks of the order of 1.1×10^5 m/s, 1.6×10^5 m/s, and 2.3×10^5 m/s are observed, respectively. It demonstrates that electron velocities display significant temporary increases (overshoots) at high electric fields before settling down to their steady-state values. This behavior arises from the difference in how quickly electrons lose momentum and energy, which varies depending on their energy level. Transient overshoot typically occurs when the applied electric field is strong enough to propel electrons into a high-energy range. In this high-energy region, electrons lose momentum more quickly than they lose energy. However, after a short time, energy loss mechanisms become dominant, causing the distribution of electron energies to broaden and the drift velocity to decrease. The average energy of electrons in Si increases at first, then it stays constant (see figure 5(b)).

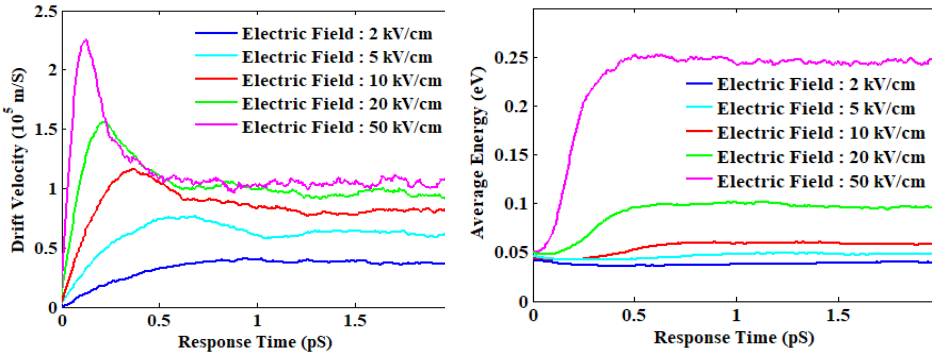

(a) (b)

Fig. 5. The time response of non-equilibrium (a) electron velocity and (b) energy in silicon at T=300K

As the applied electric field increases, the peak drift velocity reaches higher values and shifts towards shorter times. This behavior of electron drift velocity is due to the complete filling of the central valley by electrons in times less than 0.5 ps. Therefore, during this time, the probability of inter-valley scattering of electrons is lower, and consequently, the factors reducing electron velocity are fewer. Over time, electrons gain enough energy to scatter into higher-energy valleys. Due to the difference between electron momentum and relaxation time for electron transitions between valleys, which is a function of electron energy, in high electric fields (10 kV/cm, 20 kV/cm, and 50 kV/cm), it encounters velocity overshoot during inter-valley transitions. After a longer time, the electron scattering rates reach equilibrium, and the electron drift velocity and energy reach a steady state.

Figure 6 shows the electron drift velocity and average energy as a function of distance (this distance refers to the distance from the cathode to the anode). In electric fields below the threshold field, the drift velocity reaches a steady state at dimensions of 50 nm. However, for fields above the threshold, a steady state is achieved at 100 nm. Consequently, when fabricating devices with lengths larger than these values, considering the steady-state drift velocity is sufficient. However, for devices with smaller lengths, the non-steady-state behavior of electron drift velocity should be taken into account. Electron energy also experiences a transmission state along the device (see figure 6(b)).

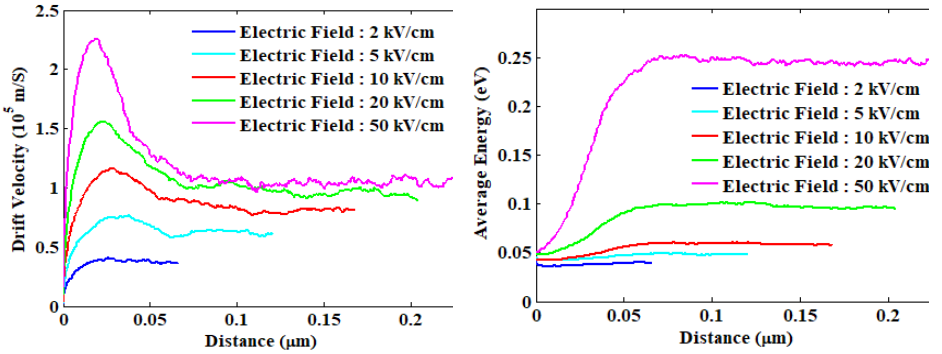

(a) (b)

Fig. 6. (a) Electron drift velocity and (b) average energy as a function of distance in silicon at 300K

Figure 7 plots the electron transit time in terms of the distance. By this finding, one can determine the necessary electric field to achieve the minimum electron transit time in devices with a given length. For instance, for a gate length of 0.10 µm, the minimum electron transit time corresponds to an electric field of 50 kV/cm. However, if it is desired to apply less power to the device, such as an electric field of 20 kV/cm, the transit time for the same gate length increases by 0.21 pS compared to the previous case, and the device performance decreases. Similarly, to design a transistor with a gate length of 0.1 µm and a transit time of 1 pS, a field on the order of 2 kV/cm should be applied to the device.

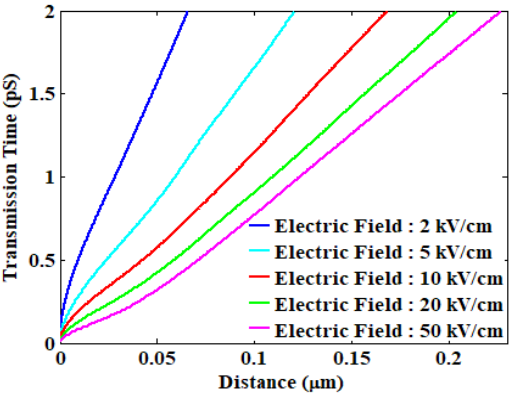

Fig. 7. The electron transit time in terms of the distance for electric fields from 2 kV/cm to 50 kV/cm at 300K

Figure 8 illustrates the energy in terms of the trajectory for three electrons for an electric field of 50 kV/cm at 300K.

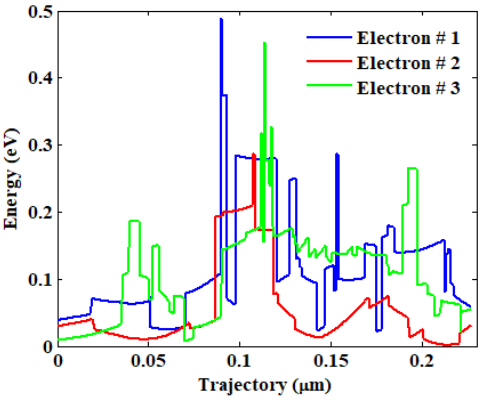

Fig. 8. The electron energies in terms of the trajectory for an electric field of 50 kV/cm at 300K

For better evaluation, the simulation results of the proposed Monte Carlo method are assessed by references [35-38], and also the Silvaco simulation in table 1. It can be seen that for different electric fields, the proposed Monte Carlo model has a good agreement with other data [35-38] and the commercial software Silvaco. The simplicity of the proposed model and its efficiency make it possible to use it as a basic and effective model for simulating silicon-based devices. Providing a microscopic picture of the movement of electrons in semiconductors

can give researchers a very good understanding so that they can better design and analyze devices made of silicon. Table 1 presents the percentage deviations of both drift velocity and average energy. While the drift velocity deviation remains below 5%, the average energy deviation reaches up to 8.4%.

Table 1. The comparison of the silicon drift velocity and average energy with references [35-38].

Reference	Model/Method	Drift Velocity ($\times 10^5$ m/s)	Deviation of Drift Velocity (%)	Electric Field (kV/cm)	Average Energy (meV)	Deviation of Average Energy (%)
[35]	Experimental	0.40	5.0	2	39.41	1.8
		0.61	3.3	5	48.76	1.6
		0.80	1.2	10	59.15	0.8
		0.95	0.0	20	99.33	0.3
		1.04	0.0	50	249.09	8.4
[36]	Drift and Diffusion Simulation	0.77	3.7	10	58.55	0.4
		0.88	2.1	20	98.43	0.1
		0.94	1.9	50	246.61	8.4
[37]	Monte Carlo Simulation	0.82	1.2	10	-	-
		1.01	2.9	50	-	-
[38]	Monte Carlo Simulation	0.79	2.5	10	-	-
		0.97	2.1	20	-	-
		1.05	1.0	50	-	-
Silvaco	Numerical Simulation	0.40	5	2	40.21	1.3
		0.60	1.7	5	50.06	3.1
		0.82	2.5	10	60.05	1.2
		0.96	1.1	20	100.01	0.9
		1.06	1.9	50	251.10	0.3
This work	Monte Carlo Simulation	0.40	-	2	39.02	-
		0.60	-	5	49.86	-
		0.81	-	10	59.91	-
		0.95	-	20	100.01	-
		1.04	-	50	250.10	-

4. CONCLUSION

This research investigates the electron transport properties in silicon semiconductors using a three-valley model and Monte Carlo simulation. The studies show a threshold field of approximately 30 kV/cm for this material.

Furthermore, the drift velocity in silicon under fields exceeding the threshold value reaches a steady state after a prolonged period. Consequently, when designing devices operating under such high fields, device dimensions should be carefully determined by analyzing the drift velocity versus device length plots and identifying the minima in electron transit time versus device length figures. Additionally, the drift velocity characteristic exhibits significant sensitivity to temperature variations, rendering silicon less suitable for electronic devices operating in environments with substantial temperature fluctuations. The findings of this research can contribute to the design of high-speed integrated circuits and provide valuable insights into the behavior of electrons in silicon under high electric fields. Moreover, the developed simulation framework establishes a versatile foundation for exploring charge transport in other material systems, such as compound semiconductors (e.g., GaAs, GaN), and for investigating quantum confinement effects in nanoscale devices.

ACKNOWLEDGMENT

This work was supported by Shahid Chamran University of Ahvaz, grant number SCU.EE1404.672.

REFERENCES

[1] O.F. Vyvenko, O. Kruger, M. Kittler, Cross-sectional electron-beam-induced current analysis of the passivation of extended defects in cast multicrystalline silicon by remote hydrogen plasma treatment. Appl. Phys. Lett. 76 (2000) 697. https://doi.org/10.1063/1.125865

[2] H. Warlimont, W. Martienssen, Springer Handbook of Condensed Matter and materials Data, Berlin: Springer, ch 4 (2005) 124. https://doi.org/10.1007/978-3-319-69743-7

[3] F. Haddadan, M. Soroosh, Low-power all-optical 8-to-3 encoder using photonic crystal-based waveguides. Photon. Net. Commun. 37 (2019) 83. https://doi.org/10.1007/s11107-018-0795-3

[4] F. Haddadan, M. Soroosh, A new proposal for 4-to-2 optical encoder using nonlinear photonic crystal ring resonators. Int. J. Opt. Photonics. 13 (2019) 119. https://doi.org/10.29252/ijop.13.2.119

[5] F. Haddadan, M. Soroosh, N. Alaei-Sheini, Designing an electro-optical encoder based on photonic crystals using the graphene–Al_2O_3 stacks. Appl. Opt. 59 (2020) 2179. https://doi.org/10.1364/AO.386248

[6] M.J. Maleki, M. Soroosh, G. Akbarizadeh, F. Parandin, F. Haddadan, Photonic Crystal Resonators in Designing Optical Decoders. J. Optoelectron. Nanostruc. 8 (2023) 1-24. https://doi.org/10.30495/jopn.2023.32220.1296

[7] M.J. Maleki, M. Soroosh, F. Parandin, F, Haddadan, Photonic Crystal-Based Decoders: Ideas and Structures In: Recent Advances and Trends in Photonic Crystal Technology, London: Intechopen, Vol 1, Ch 5, (2023) 114. https://doi.org/10.5772/intechopen.1002401
[8] F. Pakrai, M. Soroosh, J. Ganji, Designing of all-optical subtractor via PC-based resonators. J. Optoelectron. Nanostruc. 7 (2022) 21-36. https://doi.org/10.30495/JOPN.2022.29545.1246
[9] S.M.H. Jalali, M. Soroosh, G. Akbarizadeh, Ultra-fast 1-bit comparator using nonlinear photonic crystal based ring resonators. J. Optoelectron. Nanostruc. 4 (2019) 59-72. https://doi.org/20.1001.1.24237361.2019.4.3.5.7
[10] F. Haddadan, M. Soroosh, J. Singh, Designing an electro-optical 8-to-3 encoder based on resonant cavity and graphene-Al2O3 stack in the photonic crystal platform. J. Optoelectron. Nanostruc. 9(2024) 1. https://doi.org/ 10.30495/jopn.2024.33689.1328
[11] F. Haddadan, M. Soroosh, Design and simulation of a subwavelength 4-to-2 graphene-based plasmonic priority encoder. Opt. Las. Technol. 157 (2023) 108680. https://doi.org/10.1016/j.optlastec.2022.108680
[12] F. Bagheri, M. Soroosh, F. Haddadan, Y. Seifi-Kavian, Design and simulation of a compact graphene-based plasmonic D flip-flop. Opt. Las. Technol. 155 (2022) 108436. https://doi.org/10.1016/j.optlastec.2022.108436
[13] M. Soroosh, F. Parandin, F. Haddadan, M.J. Maleki, F. Bagheri, Highly efficient materials for photonic crystal-based optical components In: Advances in All-optical Communication, New York: IOP Publishing, Vol 1, Ch 1, (2024) 1. https://doi.org/10.1088/978-0-7503-5623-7ch1
[14] M. Soroosh, A. Farmani, M.J. Maleki, F. Haddadan, M. Mansouri, Highly Efficient Graphene-Based Optical Components for Networking Applications In: Photonic Crystal and Its Applications for Next Generation Systems, Springer Nature Singapore, Vol 1, Ch 2, (2023) 15. https://doi.org/10.1007/978-981-99-2548-3_2
[15] F. Haddadan, M. Soroosh, A. Basem, H.A. Kenjrawy, Nano-strip Engineering for Coupling Length Enhancement in Pattern-Free Suspended Graphene-based Plasmonic Waveguides. Plasmonics. 20 (2025) 3455. https://doi.org/10.1007/s11468-024-02541-9
[16] F. Haddadan, F. Bagheri, A. Basem, H.A. Kenjrawy, M. Soroosh, Evanescent field engineering to reduce cross-talk in pattern-free suspended graphene-based plasmonic waveguides using nano-strips. Optik. 313 (2024) 171989. https://doi.org/10.1016/j.ijleo.2024.171989
[17] M.J. Maleki, M. Soroosh, F, Haddadan, Graphene-Based Optical Waveguides for Surface Plasmon Polariton Transmission Optical Waveguide Technology and Applications In: Optical Waveguide Technology and and

Applications. London: Intechopen. Vol 1, Ch 5, (2024) 163. https://doi.org/10.5772/intechopen.114810
[18] K. Tomizawa, Numerical Simulation of Submicron Semiconductor Device, Berlin: Artech House. Vol 1, Ch 2, (1993) 31.
[19] K.K. Ng, Complete Guide to Semiconductor Devices, New York: IEEE Press. Vol 1, Ch 3, (2008) 136. https://doi.org/10.1002/9781118014769
[20] F. Haddadan, M. Soroosh, R. Rajasekar, Analysis and Simulation of the Schottky Junction Using an Ensemble Monte Carlo Model. J. Optoelectron. Nanostruc. 9 (2024) 1. https://doi.org/10.30495/JOPN.2024.33465.1318
[21] F. Haddadan, M. Soroosh, R. Rajasekar, Design and simulation of the charge layer effect on the Schottky junction characteristics using an ensemble Monte Carlo model. J. Comput. Electron. 24 (2025) 1. https://doi.org/10.1007/s10825-024-02249-3
[22] F. Haddadan, M. Soroosh, M.J. Maleki, Presenting a two-valley Monte Carlo model for simulating and analyzing electron behavior in GaAs bulk and investigating the effects of electron transitions (Gunn Effect). InThe first international conference and the seventh national conference on electrical engineering and intelligent systems. Najafabad (2024). https://civilica.com/doc/1963406/
[23] C. Jacoboni, L, Reggiani, The Monte Carlo method for the solution of charge transport in semiconductors with applications to covalent materials. Rev. Mod. Phys. 55 (1983) 645. https://doi.org/10.1103/RevModPhys.55.645
[24] S.M. Sze, Kwok K. Ng, Physics of Semiconductor Devices, New York: Wiley. Vol 1, Ch 3, (2006) 168. https://doi.org/10.1002/0470068329
[25] C. Moglestue, Monte carlo simulation of semiconductor device, London: Chapman & Hall. Vol 1, Ch 2, (1993) 57. https://doi.org/10.1007/978-94-015-8133-2
[26] Y. Ando, C. Alain, Ensemble Monte Carlo simulation for electron transport in quantum wire structures. J. Appl. Phys. 74 (1993) 3983. http://dx.doi.org/10.1063/1.354441
[27] B. Berrabah, S. Choukria, F. Souheyla, D. Sofiane, B. Benyounes, Ensemble Monte Carlo Electron Transport Simulation for GaN n+–n–n+ Diode. Trans. Electr. Electron. Mater. 2 (2021) 290. https://doi.org/10.1007/s42341-020-00237-5
[28] A. Verma, M. Z. Kauser, B. W. Lee, K. F. Brennan, P. P. Ruden, Ensemble Monte Carlo Transport Simulations for Semiconducting Carbon Nano-Tubes. AIP Conf. Proc. 772 (2005) 1049. http://dx.doi.org/10.1063/1.1994472

[29] E. Bellotti, B. K. Doshi, K. F. Brennan, J. D. Albrecht, P. P. Ruden, Ensemble Monte Carlo study of electron transport in wurtzite InN. J. Appl. Phys. 85 (1999) 916. http://dx.doi.org/10.1063/1.369211
[30] E. Pop, Monte Carlo transport and heat generation in semiconductors. Annu. Rev. Heat Transf. 17 (2014). https://doi.org/ 10.1615/AnnualRevHeatTransfer.2014007694
[31] V. Sverdlov, E. Ungersboeck, H. Kosina, S. Selberherr, Current transport models for nanoscale semiconductor devices. Mater Sci Eng R: Rep. 58 (2008) 228. https://doi.org/10.1016/j.mser.2007.11.001
[32] D. Nagy, G. Indalecio, A. J. García Loureiro, G. Espiñeira, M. A. Elmessary, K. Kalna, N. Seoane, Drift Diffusion Versus Monte Carlo Simulated ON Current Variability in Nanowire FETs. IEEE Access. 7(2019)12790. https://doi.org/ 10.1109/ACCESS.2019.2892592
[33] D. Vasileska, S.M. Goodnick, G. Klimeck, Computational Electronics: semi classical and quantum device modeling and simulation, Berlin: CRC Press. Vol 1, Ch 4, (2010) 87. https://doi.org/10.1201/b13776
[34] SILVACO INTERNATIONAL, MOCASIM User's Manual, (2020).
[35] C. Jacononi, C. Canali, G. Ottaviani, A.A. Quaranta, A Review of Some Charge Transport Properties of Silicon. Sol. Sta. Electron. 20 (2008) 77-89. http://dx.doi.org/10.1016/0038-1101(77)90054-5
[36] C. Canali, C. Jacoboni, G. Ottaviani, A. Alberigi-Quaranta, High-field diffusion of electrons in silicon. Appl. Phys. Lett. 27 (2005) 278. https://doi.org/10.1063/1.88465
[37] M.A. Omar, L. Reggiani, Drift and diffusion of charge carriers in silicon and their empirical relation to the electric field. Sol. Sta. Electron. 30 (2007) 693-697. https://doi.org/10.1016/0038-1101(87)90106-7
[38] B. Fischer, R.H. Karl, A full-band Monte Carlo model for the temperature dependence of electron and hole transport in silicon. Appl. Phys. Lett. 76 (2020) 583. https://doi.org/10.1063/1.125824